High-order harmonic generation driven by plasmonic fields: a new route towards the generation of UV and XUV photons?

2015 J. Phys.: Conf. Ser. 601 012001

(http://iopscience.iop.org/1742-6596/601/1/012001)

High-order harmonic generation driven by plasmonic fields: a new route towards the generation of UV and XUV photons?

M F Ciappina[1], J A Pérez-Hernández[2], L Roso[2], A Zaïr[3] and M Lewenstein[4,5]

[1]Max Planck Institute for Quantum Optics, Hans-Kopfermann-Str. 1, Garching D-85748, Germany
[2]Centro de Láseres Pulsados (CLPU), Parque Científico, 37185 Villamayor, Salamanca, Spain
[3]Blackett Laboratory Laser Consortium, Imperial College London, London SW7 2AZ, United Kingdom
[4]ICFO-Institut de Ciències Fotòniques, Mediterranean Technology Park, 08860 Castelldefels, Spain
[5]ICREA-Institució Catalana de Recerca i Estudis Avançats, Lluis Companys 23, 08010 Barcelona, Spain

E-mail: `marcelo.ciappina@mpq.mpg.de`

Abstract. We present theoretical investigations of high-order harmonic generation (HHG) resulting from the interaction of noble gases with different kind of temporally and spatially synthesized laser fields. These fields, based on localized surface plasmons, are produced when, for instance, a metal nanoparticle or nanostructure, is illuminated by a few-cycle laser pulse. The enhanced field, which largely depends on the geometrical shape of the metallic nanostructure, has a strong spatial dependency in a scale comparable to the one where the electron dynamics takes place. We demonstrate that the spatial nonhomogeneous character of this laser field plays an important role in the HHG process and leads to a significant increase of the harmonic cutoff energy and modifications in the electron trajectories. The use of metal nanostructures appears to be an alternative way of generating coherent XUV light with a laser field whose characteristics can be spatially synthesized locally.

1. Introduction

There exists nowadays a high demand of coherent light sources in the ultraviolet (UV) to extreme ultraviolet (XUV) spectral range. They configure fundamental tools for basic research, material science, biology, and potentially lithography [1]. One of the main obstacles is a demanding infrastructure for XUV generation and target delivery as well as its low efficiency and duty cycle. Recent experiments based on surface plasmon resonances as light enhancers could potentially solve this problem [2–4].

Field-enhanced high-order-harmonic generation (HHG) using plasmonics fields, generated starting from engineered nanostructures or nanoparticles, requires no extra amplification stages due to the fact that, by exploiting surface plasmon resonances, the incoming electric field can be enhanced by more than 20 dB (corresponding to an increase in the intensity of several orders of magnitude). As a consequence of this enhancement, the threshold laser intensity

for HHG generation in noble gases is largely exceeded and the pulse repetition rate remains unaltered. In addition, the high-harmonics radiation generated from each nanosystem acts as a pointlike source, enabling a high collimation or focusing of this coherent radiation by means of (constructive) interference. This fact opens a wide range of possibilities to spatially arrange nanostructures to enhance or shape the spectral and spatial properties of the harmonic radiation in numerous ways [2–4].

Given the nanometric size of the so-called plasmonic 'hot spots', i.e. the spatial region where the electric field reaches its highest intensity, one of the main theoretical assumptions, namely the spatial homogeneity of the driven electric field, should to be softened. Consequently, both the analytical and numerical approaches to study laser-matter processes in atoms and molecules, in particular HHG, need to be modified to treat adequately this new scenario and allow now a spatial dependence in the laser electric field. Several authors have addressed this problem recently [5–14, 20–28, 38]. As we will demonstrate, this new characteristic affects considerably the electron dynamics and its effects are rendered into the observables, in our case the HHG spectra.

In this contribution, we make a sort of brief review about HHG driven by temporally and spatially synthesized laser fields. We first describe succinctly the different theoretical tools, putting emphasis in the modifications needed to tackle this novel scenario. After we present several selected examples, where it is clear that the nohomogeneous character of the laser electric field introduces noticeable modifications both in the HHG spectra and the electron dynamics. Finally we conclude with a short summary.

2. Theory

2.1. Quantum models

Considering the dynamics of an atomic electron in a strong laser field is primarily along the direction of the field, when linearly polarized laser pulses are employed, it is justifiable to model the HHG in a 1D spatial dimension by solving the so-called Time Dependent Schrödinger Equation (1D-TDSE) [7]. In order to model an atom in 1D, it is common to use the so-called soft core potentials, which are of the form $V_{\text{atom}}(x) = -1/\sqrt{x^2 + a^2}$, where the parameter a allow us to modify the ionization potential of the ground state, fixing it as close as possible to the value of the atom under consideration. The potential due to the laser electric field, linearly polarized along the x axis, is formulated in the dipole approximation and it is modified in order to treat spatially nonhomogeneous fields. As a consequence we write, $V_{\text{laser}}(x,t) = E(x,t)x$ where $E(x,t)$ is the laser electric field and now we can include any spatial variation (for details see e.g. [7]). The 1D-TDSE can be solved numerically by using the Crank-Nicolson scheme in order to obtain the time propagated electronic wavefunction $\Psi(x,t)$. Once $\Psi(x,t)$ is found, we can calculate the harmonic spectrum by computing the Fourier transform of the dipole acceleration of the active electron. One of the main advantages of the 1D-TDSE is that we are able to include any functional form for the spatial variation of the plasmonic field. For instance, we have implemented linear [7] and real (parabolic) plasmonic fields [7], as well as near-fields with exponential decay [25]. For all the cases we have observed noticeable differences in the HHG spectra as we will show in Section 3.

A natural extension of the above described approach is to solve the TDSE in its full dimensionality and to include in the laser-electron potential the spatial variation of the laser electric field. For only one active electron we need to deal with 3 spatial dimensions and, due to the cylindrical symmetry of the problem, we are able to separate the electronic wavefunction in spherical harmonics, Y_l^m, and take into account only terms with $m = 0$. Typically several hundreds of angular momenta l should to be considered and we could recognize the time evolution of each of them as a 1D problem. We use a Crank-Nicolson method implemented on a splitting of the time-evolution operator that preserves the norm of the wave function for

the time propagation, similar to the 1D-TDSE case. We base our studies in helium because a majority of experiments in HHG are carried out in noble gases, but other atoms could be easily implemented. After time propagation of the electronic wavefunction, the HHG spectra can be computed in an analogous way as in the case of the 1D-TDSE. Due to the complexity of the problem, we were able to carry out studies only with nonhomogeneous fields with linear spatial variations in the 3D-TDSE, but this example is enough to confirm how a spatial nonhomogeneous field strongly modifies the HHG spectra (for more details see [14]).

2.2. Semiclassical approach

An alternative approach to compute high-harmonic spectra for atoms in intense laser pulses is the Strong Field Approximation (SFA) or Lewenstein model [39]. The main ingredient of this approach is the evaluation of the time-dependent dipole moment $\mathbf{d}(t)$. Within the single active electron (SAE) approximation it can be calculated starting from the ionization and recombination transition matrices combined with the classical action of the laser-ionized electron moving in the laser field. The SFA approximation has a direct interpretation in terms of the so-called three-step or simple man's model [39]. The first step is the strong-field ionization of the atom or molecule as a consequence of the nonperturbative interaction with the coherent electromagnetic radiation. Next, the classical movement of the electron in the laser electric field defines the second step of the model. Finally, the third step in the sequence arises when the laser-ionized electron is steered back to its origin, due to the inversion in the direction of the laser electric field, recombining with the parent ion under the emission of a high-energy photon. One of the main features of the HHG process is the coherence of the emitted radiation, which, amongst other uses, opens the possibility of generating attosecond pulses [1]. Implicitly the Lewenstein model deals with spatially homogeneous electric and vector potential fields, i.e. fields that do not experience variations in the region where the electron dynamics takes place. In order to consider spatially nonhomogeneous fields, the SFA approach needs to be modified accordingly, i.e. the ionization and recombination transition matrices, joint with the classical action, should to take into account this new feature of the laser field (for further details see [7,8]).

2.3. Classical framework

Relevant information, for instance the HHG cutoff and properties of the electron trajectories, can be obtained solving the classical Newton-Lorentz equation for an electron moving in a linearly polarized electric oscillating field, i.e. using fully classical considerations. The following conditions are commonly set (the resulting model is also known as the simple man's model): i) the electron starts with zero velocity at the origin at time $t = t_i$, defining the ionization time t_i, i.e., $x(t_i) = 0$ and $\dot{x}(t_i) = 0$; (ii) when the laser electric field reverses its direction, the electron returns to its initial position, i.e., recollides with the parent ion, at a later time, $t = t_r$ (the so-called recollision time), i.e. $x(t_r) = 0$. The kinetic energy of the laser-ionized electron at the recollision (return) time t_r can be obtained from the usual formula $E_k(t_r) = \dot{x}(t_r)^2/2$, and, finding the value of t_r (as a function of t_i) that maximizes this energy, we find that the HHG cutoff holds $n_c\omega = 3.17U_p + I_p$, where n_c is the harmonic order at the cutoff, ω is the laser frequency, U_p is the ponderomotive energy ($U_p = I/4\omega^2$, with I being the laser intensity in a.u.), and I_p is the ionization potential of the atom or molecule under consideration. It is worth of mention that the HHG cutoff will be extended when spatially inhomogeneous fields are employed as we will see in Section 3. We have solved numerically the Newton equation for an electron moving in a linearly polarized (in the x-axis) electric field with the same parameters used in the quantum models in order to compare the outcomes of both (see Section 3). Specifically, we find the numerical solution of $\ddot{x}(t) = -\nabla_x V_{\text{laser}}(x,t)$ where $V_{\text{laser}}(x,t)$ was defined in Section 2.1. For fixed values of ionization times t_i, it is possible to obtain the classical trajectories and to numerically calculate the times t_r for which the electron recollides with the parent ion. In

addition, once the ionization time t_i is fixed, the full electron trajectory is completely determined (for more details about the classical model see [28]).

3. Selected results

In the following sub-sections we present a brief summary of the results reported in several articles published recently. In these works, different noble gases (He, Ar and Xe) are used as atomic targets located in the vicinity of metal nanotips and nanoparticles and the HHG generated by them was studied and characterized.

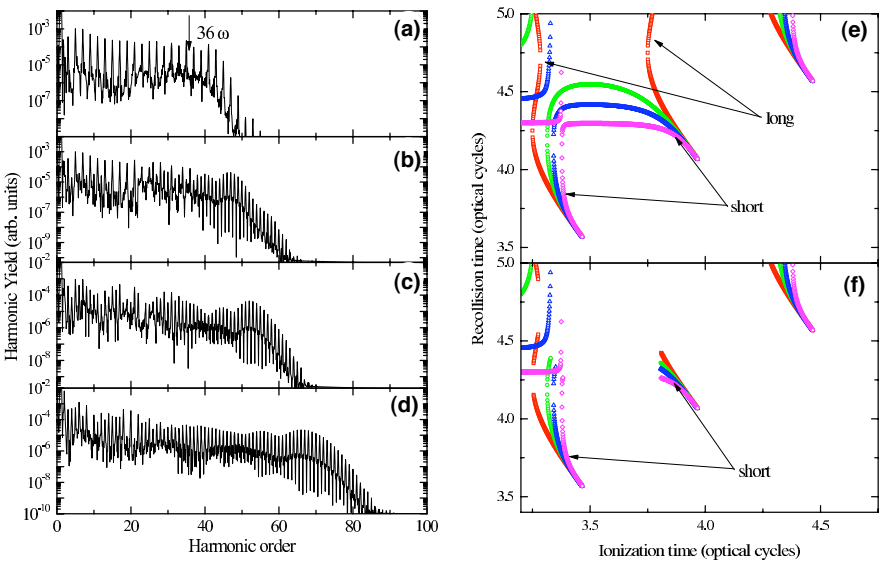

Figure 1. HHG spectra for a model atom with a ground-state energy, $\mathcal{E}_{\rm GS} = -0.67$ a.u. generated using the 1D-TDSE approach. The laser parameters are $I = 2 \times 10^{14}$ W·cm^{-2} and $\lambda = 800$ nm. We have used a trapezoidal shaped pulse with two optical cycles turn on, i.e. $n_{\rm on} = 2$, and turn off, i.e. $n_{\rm off} = 2$, and a plateau with six optical cycles, i.e. $n_{\rm p} = 6$ (10 optical cycles in total, i.e. approximately 27 fs). The arrow indicates the cutoff predicted by the semiclassical model [39]. Panel (a): homogeneous case, (b): $\varepsilon = 0.01$ (100 a.u), (c): $\varepsilon = 0.02$ (50 a.u) and (d): $\varepsilon = 0.05$ (20 a.u). The parameter ε controls the *strength* of the inhomogeneity and for the linear case has dimension of inverse length. The values between brackets correspond to the inhomogeneity regions (see [7] for more details). In panels (e) and (f) is shown the dependence of the semiclassical trajectories on the ionization and recollision times for different values of ε and for the non confined case, panel (e) and the confined case, panel (f), respectively. Red squares: homogeneous case $\varepsilon = 0$; green circles: $\varepsilon = 0.01$; blue triangles: $\varepsilon = 0.02$ and magenta diamonds: $\varepsilon = 0.05$. This figure has been adapted from [7].

3.1. HHG driven by spatially (linear) nonhomogeneous fields and electron confinement

In this sub-section we summarize the study carried out in [7] where it is shown that both the inhomogeneity of the local fields and the confinement of the electron movement, play an important role in the HHG process and lead to the generation of even harmonics and a significant increase in the HHG cutoff, more pronounced for the longer wavelengths cases studied. In order to understand and characterize these new HHG features we employ two of the different approaches mentioned above: the numerical solution of the 1D-TDSE (see panels (a)-(d) in

Fig. 1) and the semiclassical approach known as Strong Field Approximation (SFA). Both approaches predict comparable results and reproduce satisfactorily the new features, but by employing the semiclassical arguments (see panels (e) and (f) in Fig. 1) behind the SFA and time-frequency analysis tools (Fig. 2), we are able to fully understand the reasons of the cutoff extension. A more detailed study can be found in [7].

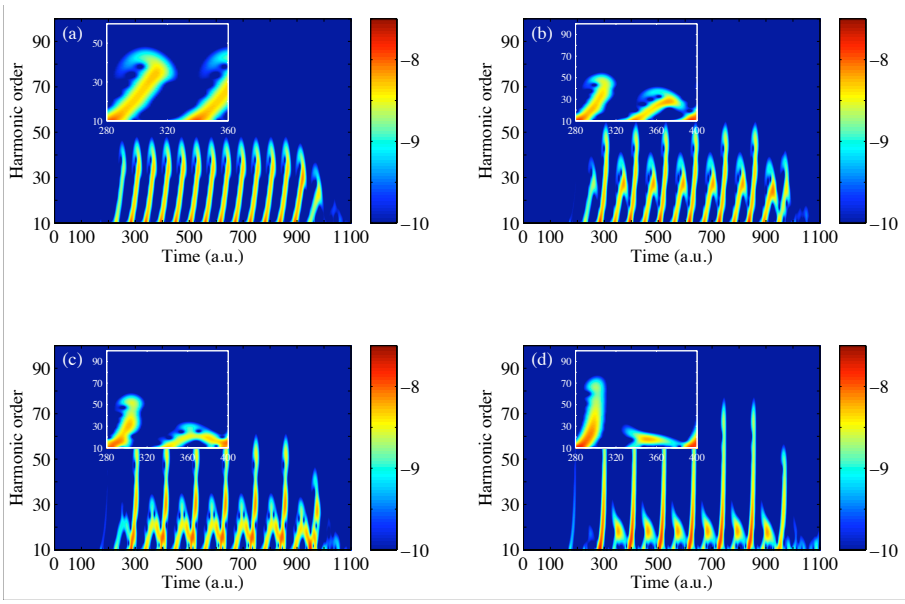

Figure 2. Panels (a)-(d): Gabor analysis for the corresponding HHG spectra of panels (a)-(d) of Fig. 1. The zoomed regions in all panels show a time interval during the laser pulse for which the complete electron trajectory, from birth time to recollision time, falls within the pulse plateau. In panels (a)-(d) the color scale is logarithmic. This figure has been adapted from [7].

3.2. HHG driven by real nonhomogeneous fields

In this sub-section we include numerical simulations of HHG in Ar produced by the fields generated when a gold bow-tie nanostructure is illuminated by a short laser pulse of long wavelength (see [9] for more details). The functional form of these fields is extracted from finite element simulations using both the complete geometry of the metal nanostructure and the laser pulse characteristics (see Fig. 3(a)). We use the numerical solution of the TDSE in reduced dimensions to predict the HHG spectra. We observe an extension in the harmonic cutoff position that could lead to the production of XUV coherent laser sources and open the avenue to the generation of attosecond pulses. It is shown in Fig. 3(c) that this new feature is a consequence of the combination of a spatial nonhomogeneous electric field, which modifies substantially the electron trajectories, and the confinement of the electron dynamics. Furthermore, our numerical results are supported by time-analysis and classical simulations. A more pronounced increment in the harmonic cutoff, in addition with an appreciable growth in the conversion efficiency, could be attained optimizing the nanostructure geometry and by choosing the adequate materials. These degrees of freedom could pave the way to tailor the harmonic spectra according to specific requirements.

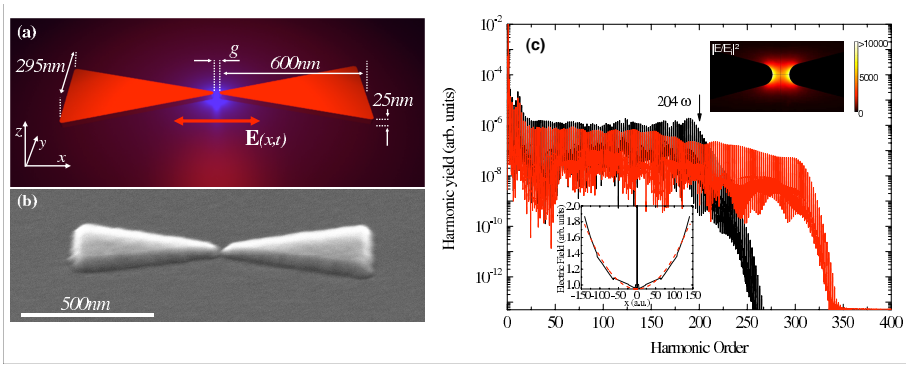

Figure 3. (a) Schematic representation of the geometry of the considered nanostructure. A gold bow-tie antenna resides on a glass substrate (refractive index $n = 1.52$) with superstate medium of air ($n = 1$). The characteristic dimensions of the system and the coordinate system used in the 1D-TDSE simulations are shown. (b) SEM image of a real gold bow-tie antenna. (c) High-order harmonic generation (HHG) spectra for Ar (Ionization potential $\mathcal{E}_{\rm GS} = -0.58$ a.u.), driven by a laser pulse with wavelength $\lambda = 1800$ nm and intensity $I = 1.25 \times 10^{14}$ W·cm^{-2} at the center of the gap $x = 0$. We have used a trapezoidal shaped pulse with three optical cycles turn on, i.e. $n_{\rm on} = 3$, and turn off, i.e. $n_{\rm off} = 3$, and a plateau with four optical cycles, i.e. $n_{\rm p} = 4$ (about 60 fs). The gold bow-tie nanostructure has a gap $g = 15$ nm (283 a.u.). The black line indicates the homogeneous case while the red line indicates the nonhomogeneous case. The arrow indicates the cutoff predicted by the semiclassical model for the homogeneous case [39]. The top left inset shows the functional form of the electric field $E(x,t)$, where the solid lines are the raw data obtained from the finite element simulations and the dashed line is a nonlinear fitting. The top right inset shows the intensity enhancement in the gap region of the gold bow-tie nanostructure. This figure has been adapted from [9].

3.3. HHG driven by temporal and spatial synthesized fields

In this sub-section we present a brief report of the results published in [14]. In short, numerical simulations of HHG in He atoms using a temporal and spatially synthesized laser field are considered using the full 3D-TDSE. The field resulting from both time and space synthesis, provides a new route for the generation of photons at energies beyond the carbon K-edge using $\lambda = 800$ nm laser pulses, which can be obtained from conventional Ti:Sapphire laser sources, now relatively common amongst the strong field physics community. The temporal synthesis is performed using two few-cycle laser pulses delayed in time [15]. Few-cycle laser pulses are now routinely used for attoscience applications and are produced using a post-compression stage [16, 17]. The spatial synthesis is obtained by using a nonhomogeneous laser field [5–7] produced when a laser beam is focused in the vicinity of a metal nanostructure or nanoparticle. In particular, the temporal synthesized laser field is described by $E_1(t) = E_0 \sin^2\left(\frac{\omega t}{2N}\right)\sin(\omega t)$ and $E_2(t,\tau) = E_0 \sin^2\left(\frac{\omega(t-\tau)}{2N}\right)\sin(\omega(t-\tau)+\phi)$ where E_0 is the laser electric field amplitude in atomic units ($E_0 = \sqrt{I/I_0}$ with $I_0 = 3.5 \times 10^{16}$ W/cm^2), $\omega = 0.057$ a.u. the laser frequency corresponding to $\lambda = 800$ nm, T the laser period, N the total number of cycles in the pulse, ϕ the carrier-envelope phase (CEP) and τ the time delay between the pulses. We consider the case $N = 4$ and $\phi = 0$ and $\tau = 1.29T$ (see [15] for more details). It is worth to mention, however, that there exists another complementary ways to perform the temporal synthesis, for instance, using chirped input laser pulses [18, 19].

Regarding the spatial synthesis, the nonhomogeneous spatial distribution of the laser field can be obtained experimentally by using the laser field as produced by nano-plasmonic

antennas [2, 5–7], metallic waveguides [3], metal [29, 30] and dielectric nanoparticles [31] or metal nanotips [32–36]. The main feature of these fields is that they are no longer spatially homogeneous in the region where the electron dynamics takes place. Very recently, studies about how HHG spectra are modified due to spatial nonhomogeneous fields have been published [5–7,9] leading to the so-called 'HHG driven by resonant plasmon field enhancement' showing the growing interest of such new subject.

The coupling between the atom and the laser pulse, linearly polarized along the z axis, is modified in order to treat spatially nonhomogeneous fields as: $V_{\text{laser}}(z,t,\tau) = \tilde{E}(z,t,\tau)\, z$, with $\tilde{E}(z,t,\tau) = E(t,\tau)(1+\beta z)$, where $V_{\text{laser}}(z,t,\tau)$ represents the laser-atom interaction in the length gauge and $E(t,\tau) = E_1(t) + E_2(t,\tau)$ is the temporal synthesized laser field. The parameter β defines the strength of the nonhomogeneity and the dipole approximation is preserved because $\beta \ll 1$.

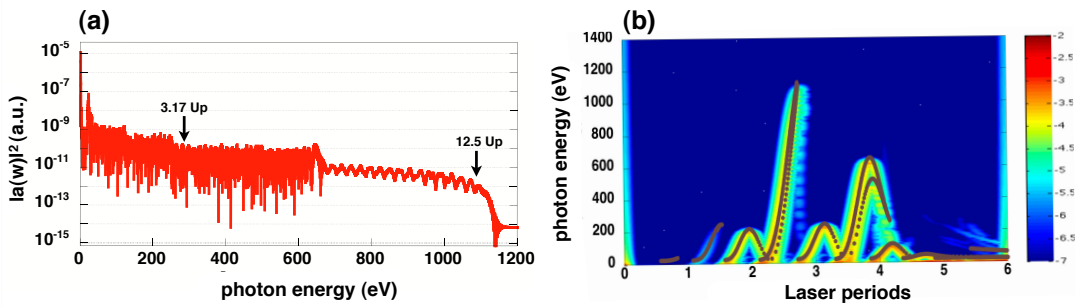

Figure 4. (a) 3D-TDSE harmonic spectrum for a He atom driven by the spatially and temporally synthesized pulse described above with $\beta = 0.002$. The plasmonic enhanced intensity is $I = 1.4 \times 10^{15}$ W/cm^2. (b) Time-frequency analysis obtained from the 3D-TDSE and superimposed (in brown) with the classical rescattering energies for the same parameters used in (a). This figure has been adapted from [14].

The linear functional form for the spatial nonhomogeneity described above could be obtained by engineering adequately the geometry of plasmonic nanostructures and adjusting the laser parameters in such a way that the laser-ionized electron feels only a linear spatial variation of the laser electric field when in the continuum (see e.g. [9] and references therein). The harmonic spectrum then obtained in He for $\beta = 0.002$ is presented in Fig. 4(a). We can observe a considerable cut-off extension up to $12.5U_p$ which is much larger when compared with the double pulse configuration employed alone (it leads only to a maximum of $4.5U_p$ [15]). This large extension of the cut-off is therefore a signature of the combined effect of the double pulse and the spatially nonhomogeneous character of the laser electric field. For this particular value of the laser peak intensity (1.4×10^{15} W/cm^2) the highest photon energy is greater than 1 keV. Note that the quoted intensity is actually the plasmonic enhanced intensity, not the input laser intensity. The latter could be several orders of magnitude smaller, according to the plasmonic enhancement factor (see e.g. [2,3]) and will allow the nanoplasmonic target to survive to the interaction with the incoming laser pulse. In order to confirm the underlying physics highlighted by the classical trajectories analysis, we retrieved the time-frequency distribution of the calculated dipole (from the 3D-TDSE) corresponding to the case of the spectra presented in Fig. 4(a) using a wavelet analysis. The result is presented in Fig. 4(b) where we have superimposed the calculated classical rescattering energies (in brown) to show the excellent agreement between the two theoretical approaches. The consistency of the classical calculations with the full quantum approach is clear and confirms the mechanism of the generation of

this $12.5U_p$ cut-off extension. In addition, the HHG spectra exhibit a clean supercontinuum as a result of the trajectory selection on the recollision time, consequences of employing the combination of a temporally and spatially synthesized laser field.

3.4. HHG driven by plasmonic near-fields

This sub-section includes a brief summary of the results reported in [20]. In such contribution it is shown how the HHG spectra from Xe atoms are modified by using a plasmonic enhanced near-field generated when a metal nanoparticle is illuminated by a short laser pulse. We use the function given by [30] to define the spatial nonhomogeneous laser electric field $E(x,t)$, i.e. $E(x,t) = E_0\, f(t)\, \exp(-x/\chi) \sin(\omega t + \phi)$ where E_0, ω, $f(t)$ and ϕ are the peak amplitude, the laser field frequency, the field envelope and the phase, respectively. The functional form of the resulting laser electric field is extracted from attosecond streaking experiments and incorporated both in our quantum and classical mechanical approaches. In this specific case the spatial dependence of the plasmonic near-field is given by $\exp(-x/\chi)$ and it depends on both the size and the material of the spherical nanoparticle used. $E(x,t)$ is valid for x outside of the metal nanoparticle, i.e. $x \geq R_0$, where R_0 is its radius and it is important to note that the electron motion stands in the region $x \geq R_0$ with $(x + R_0) \gg 0$. We consider the laser field having a $\sin^2$ envelope: $f(t) = \sin^2\left(\frac{\omega t}{2n_\mathrm{p}}\right)$, where n_p is the total number of optical cycles, i.e. the total pulse duration is $\tau = 2\pi n_\mathrm{p}/\omega$. The harmonic yield of the atom is obtained by Fourier transforming the dipole acceleration $a(t)$ of the electronic wavepacket.

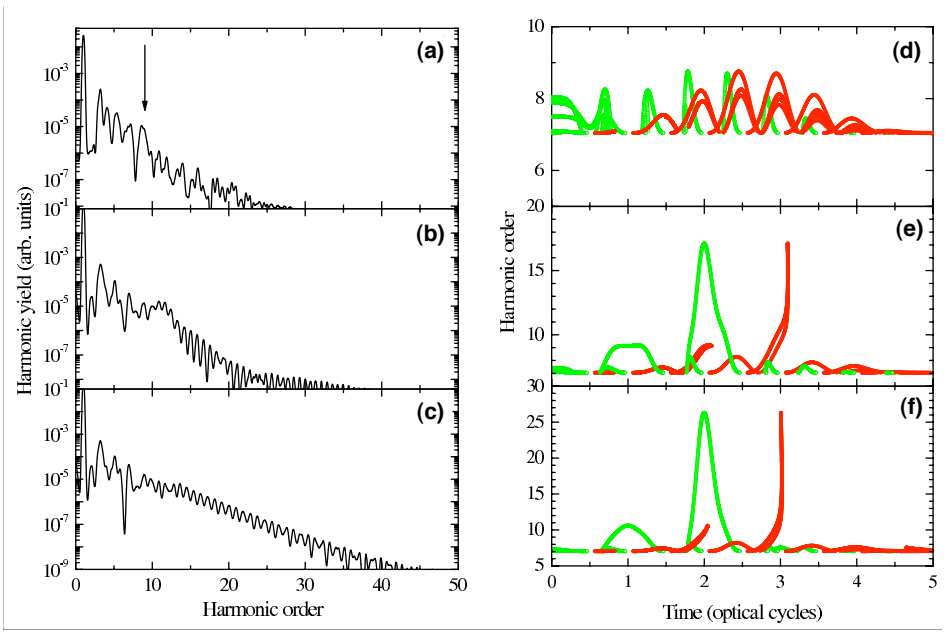

Figure 5. HHG spectra for Xe, laser wavelength $\lambda = 720$ nm and intensity $I = 2 \times 10^{13}$ W·cm^{-2}. We use a $\sin^2$ shaped pulse with $n_\mathrm{p} = 5$. Panel (a) shows the homogeneous case, panel (b) $\chi = 50$ and panel (c) $\chi = 40$. The arrow in panel (a) indicates the cut-off predicted by the semiclassical model [39]. Panels (d)-(f) represent the corresponding total energy of the electron (expressed in harmonic order) driven by the laser field calculated from Newton's second law and plotted as a function of the t_i (green (light gray) circles) or the t_r (red (dark gray) circles). This figure has been adapted from [20].

Figure 5 panels (a)-(c) depict the harmonic spectra for Xenon generated by a laser pulse with $I = 2 \times 10^{13}$ W/cm^2, $\lambda = 720$ nm and a $\tau = 13$ fs, i.e $n_{\rm p} = 5$ (this pulse corresponds to an intensity envelope of ≈ 4.7 fs FWHM) [30]. For the case of a homogeneous field no harmonics beyond the 9$^{\rm th}$ order are observed. The spatial decay constant χ quantifies the nonhomogeneity due to the nanoparticle and it varies together with its size and the material (metal) employed. Changing χ is therefore equivalent to choosing the type of nanoparticle used, which leads to overcome the semiclassically predicted cutoff limit and reach higher harmonic orders. For instance with $\chi = 40$ and $\chi = 50$ harmonics in the mid 20s (panel c) and well above the 9$^{\rm th}$ (a clear cut-off at $n_c \approx 15$ is visible) (panel b), respectively, are observed. A change in the harmonic periodicity, related to the breaking of symmetry imposed by the induced non-homogeneity, is clearly visible as well.

We now consider the semiclassical simple man's (SM) model [37, 39] in order to characterize the harmonic cut-off extension. This new feature may appear due to the combination of several factors (for details see [7, 9]). It is well established that $n_c = (3.17U_p + I_p)/\omega$, where n_c is the harmonic order at the cut-off and U_p the ponderomotive energy. We solve numerically the Newton-Lorentz equation for an electron moving in an oscillating electric field with the same parameters used in the TDSE-1D calculations, i.e. $\ddot{x}(t) = -\nabla_x V_{\rm laser}(x,t) = -E(x,t)(1 - \frac{x(t)}{\chi})$, and consider the SM model initial conditions: the electron starts at position zero at $t = t_i$ (the ionization time) with zero velocity, i.e. $x(t_i) = 0$ and $\dot{x}(t_i) = 0$. When the laser electric field reverses its direction, the electron returns to its initial position (i.e. the electron *recollides* or recombines with the parent ion) at a later time $t = t_r$ (the recollision time), i.e. $x(t_r) = 0$. The electron kinetic energy at the t_r is calculated from: $E_k(t_r) = \frac{\dot{x}(t_r)^2}{2}$ and finding the t_r (as a function of t_i) that maximizes E_k, n_c is also maximized.

In panels (d)-(f) of Fig. 5 we show the dependence of the harmonic order upon the t_i and t_r, calculated from $n = (E_k(t_{i,r}) + I_p)/\omega$ as for the cases (a)-(c) of Fig. 5, respectively. Panels (a), (b) and (c) depict the cases of ($\chi \to \infty$) (homogeneous field), $\chi = 50$ and $\chi = 40$, respectively. Panels (b) and (c) show how the nonhomogeneity character of the laser field modifies considerably the electron trajectories towards an extension of the n_c. Limits clearly present at $n_c \sim 18\omega$ (28 eV) and $n_c \sim 27\omega$ (42 eV) for $\chi = 50$ and $\chi = 40$, respectively, are observed. These last two cut-off values are indeed consistent with the quantum mechanical calculations presented in panels (b) and (c) of Fig. 5.

Both models, classical and quantum, report an extension in the n_c position that could lead to the production of XUV coherent laser sources and opening the avenue to the generation of attosecond pulses. This new feature is a consequence of the induced laser field nonhomogeneity only, which modifies substantially the electron trajectories. A more pronounced increment in the harmonic cut-off, in addition with an appreciable growth in the conversion efficiency, could be reached varying, for instance, both the radius and the material (metal) of the spherical nanoparticles. These new degrees of freedom could pave the way to enhance the harmonic spectra reaching the XUV regime with modest input laser intensities.

4. Conclusions

We studied high-order-harmonic generation (HHG) driven by temporal and spatial synthesized fields. These fields are not merely a theoretical speculation but are present in a vicinity of a metal nanostructure or nanoparticle, of nanometric dimensions, when it is illuminated by a short and intense laser pulse. We have shown several prominent examples where it is possible to infer that the spatial nonhomogeneous character of the laser electric field introduces a new degree of freedom, which, manipulated adequately, could open the possibility to generate efficiently coherent radiation in the UV and XUV range. Regarding the experimental feasibility, important challenges still remains about the possibility to achieve high energetic photons via spatial nonhomogeneous fields and, in some aspects this is not free of controversy [40]. However,

we would like to stress out that the theory envisions that this process is physically feasible. Our predictions are based on the convergence of three different approaches, quantum, semiclassical and classical, and consequently the robustness of our results appears to be settled.

Acknowledgments
We acknowledge the financial support of the ERC Advanced Grants QUAGATUA and OSYRIS, Alexander von Humboldt Foundation (M L); J A P-H. and L R acknowledge support from Laserlab-Europe (Grant No. EU FP7 284464) and the Spanish Ministerio de Economía y Competitividad (FURIAM Project FIS2013-47741-R). This research has been partially supported by Fundació Privada Cellex. M F C acknowledges Ferenc Krausz for useful comments and suggestions.

References

[1] Krausz F and Ivanov M 2009 *Rev. Mod. Phys.* **81** 163
[2] Kim S et al 2008 *Nature (London)* **453** 757
[3] Park I-Y et al 2011 *Nat. Phot.* **5** 677
[4] Pfullmann N et al 2013 *New J. Phys.* **15** 093027
[5] Husakou A et al 2011 *Phys. Rev. A* **83** 043839
[6] Yavuz I et al 2012 *Phys. Rev. A* **85** 013416
[7] Ciappina M F et al 2012 *Phys. Rev. A* **85** 033828
[8] Shaaran T et al 2012 *Phys. Rev. A* **86** 023408
[9] Ciappina M F et al 2012 *Opt. Express* **20** 26261
[10] Ciappina M F et al 2012 *Phys. Rev. A* **86** 023413
[11] Shaaran T et al 2012 *J. Mod. Opt.* **59** 1634
[12] Shaaran T et al 2013 *Ann. Phys. (Berlin)* **525** 97
[13] Fetić B et al 2013 *Ann. Phys. (Berlin)* **525** 107
[14] Pérez-Hernández J A et al 2013 *Phys. Rev. Lett.* **110** 053001
[15] Pérez-Hernández J A et al 2009 *J. Phys. B* **42**, 134004
[16] Sansone G et al 2006 *Science* **314**, 443
[17] Eckle P et al 2008 *Nat. Phys.* **4** 565-570
[18] Carrera J J et al 2006 *Phys. Rev. A* **74** 023404
[19] Yang Y-Y et al 2012 *Opt. Express* **21** 2195
[20] Shaaran T et al 2013 *Phys. Rev. A* **87** 041402
[21] Shaaran T et al 2013 *Phys. Rev. A* **87** 053415
[22] Yavuz I 2013 *Phys. Rev. A* **87** 053815
[23] Ciappina M F et al 2013 *Phys. Rev. A* **87** 063833
[24] Luo J et al 2013 *J. Phys. B* **46** 145602
[25] Ciappina M F et al 2013 *Laser Phys. Lett.* **10** 105302
[26] Ciappina M F et al 2014 *Phys. Rev. A* **89** 013409
[27] Feng L Q et al 2013 *Phys. Plasmas* **20** 122307
[28] Ciappina M F et al 2014 *Comp. Phys. Comm.* **185** 398
[29] Zherebtsov S et al 2011 *Nat. Phys.* **7** 656
[30] Süßmann F and Kling M F 2011 *Proc. of SPIE* **8096** 80961C
[31] Süßmann F and Kling M F 2011 *Phys. Rev B* **84** 121406(R)
[32] Hommelhoff P et al 2006 *Phys. Rev. Lett.* **96** 077401
[33] Schenk M et al 2010 *Phys. Rev. Lett.* **105** 257601
[34] Krueger M et al 2011 *Nature (London)* **475** 78
[35] Krueger M et al 2012 *J. Phys. B* **45**, 074006
[36] Herink G et al 2012 *Nature (London)* **483**
[37] Corkum P B 1993 *Phys. Rev. Lett.* **71** 1994
[38] Husakou A and Herrmann J 2014 *Phys. Rev. A* **90** 023831
[39] Lewenstein M et al 1994 *Phys. Rev. A* **49** 2117
[40] Sivis M et al 2012 *Nature (London)* **485** E1-E3